Transport and invariant manifolds near L_3 in the Earth-Moon Bicircular model

Àngel Jorba and Begoña Nicolás
Departament de Matemàtiques i Informàtica
Barcelona Graduate School of Mathematics (BGSMath)
Universitat de Barcelona (UB)
Gran Via de les Corts Catalanes 585, 08007 Barcelona, Spain
E-mails: angel@maia.ub.es, bego@maia.ub.es

31st January 2020

Abstract

This paper focuses on the role of L_3 to organise trajectories for a particle going from Earth to Moon and viceversa, and entering or leaving the Earth-Moon system. As a first model, we have considered the planar Bicircular problem to account for the gravitational effect of the Sun on the particle. The first step has been to compute a family of hyperbolic quasi-periodic orbits near L_3. Then, the computation of their stable and unstable manifolds provides connections between Earth and Moon, and also generates trajectories that enter and leave the Earth-Moon system. Finally, by means of numerical simulations based on the JPL ephemeris we show that these connections can guide the journey of lunar ejecta towards the Earth.

Contents

1 Introduction

The dynamics of a particle in the Earth-Moon system has been widely studied, however a big amount of questions remain unanswered. The work presented here is devoted to a better understanding of the natural orbits in the surroundings of Earth and Moon, generated by the collinear point L_3. Different models for analysing the motion of such a particle are found in the literature. One of the most simple and extended ones is the well known Restricted Three Body Problem (RTBP) that describes a massless particle moving under the gravitational effect of two point masses, called primaries, that revolve in circular motion around their barycentre. In this model it is usual to define the mass unit as the sum of the masses of the primaries, the longitude unit as the distance between them, and the unit of time such that the period of their circular movement is 2π. With these considerations, the universal gravitational constant becomes one. In our case, we consider that the primaries Earth and Moon, with total mass 6.0457×10^{24} kg. As, in this model, they move in circular orbits we assume that they are separated by a constant distance of 3.8440×10^5 km and revolve with constant angular velocity equal to $2\pi/27.31$ days^{-1}.

Another common consideration is to write the equations of motion in a rotating frame, also called synodic, so that the axis move along with the two primaries. In this way, primaries are seen as static points: the Earth, with mass $1-\mu$, placed at μ and the Moon, with mass μ placed at $\mu - 1$, being $\mu = 0.012150582$ the mass parameter for the Earth-Moon system.

Taking all this into account, the equations of motion of the RTBP can be written in Hamiltonian form. We will restrict the motion of the particle to the Earth-Moon plane. It is not difficult to see that the Hamiltonian system is autonomous and can be written as follows,

$$H_{RTBP} = \frac{1}{2}(p_x^2 + p_y^2) + yp_x - xp_y - \frac{1-\mu}{r_{PE}} - \frac{\mu}{r_{PM}}, \tag{1}$$

being r_{PE} and r_{PM} the distances from Earth and Moon to the particle, respectively.

It is well-known that the RTBP, in synodical coordinates, has five equilibrium points. Three of them, called collinear points (L_1, L_2 and L_3), are disposed along the horizontal axis and the other two are called equilateral or triangular points (L_4 and L_5) and are located in the third vertex of the two equilateral triangles formed by taking the primaries as vertices, see Figure 1 (left). Collinear points are unstable (they are of the form centre×saddle) while triangular equilibrium points are, for the mass ratio of the Earth-Moon system, linearly stable.

The classical Lyapunov Centre Theorem states that under generic non-resonance and non-degeneracy conditions, there exists a one-parametric family of periodic orbits emanating from each linearly stable direction of an equilibrium point of a Hamiltonian system. These families of periodic orbits have been computed extensively in the literature due to their interest in space science, see for instance the early work of R. Broucke [Bro68].

An important characteristic of the RTBP is that it conserves energy; this has the advantage of reducing one degree of freedom, but at the same time, it restricts the movements of the particle to an energy level. A modification of the RTBP that introduces the effect of a fourth body as a time periodic force is the so-called Bicircular Problem (BCP), [Hua60, CRR64]. In our case, the fourth body is the Sun: we assume that the Earth-Moon keep moving as in the RTBP, and that their barycentre revolves around the Sun-(Earth+Moon) barycentre in circular motion. Using the same reference frame and units as in the RTBP, the BCP can be seen as a perturbation of the RTBP (see Figure 1) (right). Note that this model is not coherent since the effect of the Sun on the two primaries is not taken into account, nevertheless this model is considered to give a good insight into the dynamics of the system [SGJM95]. It is also remarkable that some results

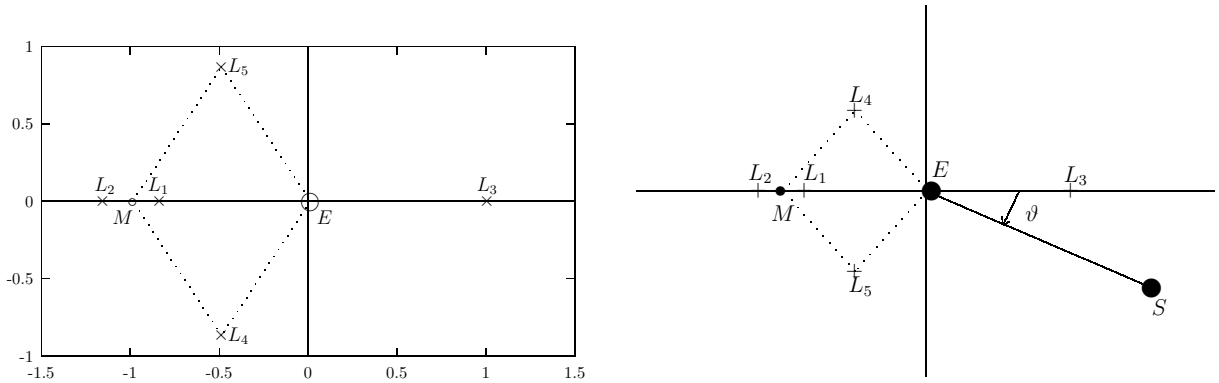

Figure 1: Schematic of the Restricted Three Body Problem (left) and of the Bicircular Model (right). Note that distance to Sun is not in scale.

μ	m_s	ω_s	a_s
0.012150582	328900.549999999	0.925195985	388.811143023

Table 1: Parameters of the Bicircular model for the Earth-Moon system, in RTBP units.

obtained using BCP model have been checked successfully using a realistic model based on the JPL ephemeris [GLMS01], [Jor00].

The BCP is still described by a Hamiltonian system, that now depends on time in a periodic way. Therefore, the energy is not conserved. Usually the Hamiltonian function describing the planar BCP is written in two parts,

$$H_{BCP} = H_{RTBP} + \hat{H}_{BPC} \tag{2}$$

where H_{RTBP} is the RTBP Hamiltonian (1), and $\hat{H}_{BCP}$ comprises the terms related to the effect of the Sun,

$$\hat{H}_{BCP} = -\frac{m_s}{r_{PS}} - \frac{m_s}{a_s^2}(y\sin(\vartheta) - x\cos(\vartheta)),$$

being r_{PS} the distance from the Sun to the particle, m_s is the Sun mass, a_s is the distance between the Sun and the Earth-Moon barycentre, $\vartheta = \omega_s t$ is the angle that specifies the position of the Sun at each time t and ω_s is the Sun angular velocity with respect to the Earth-Moon system. Table 1 contains the values of the parameters for Earth-Moon-Sun BCP in the RTBP units.

It is also well-known that the BCP preserves the symmetry when inverting the time, also found for RTBP. This means that, for a fixed value of μ, if (x, y, p_x, p_y, t) is a particular solution of the system, then $(x, -y, -p_x, p_y, -t)$ is also a solution.

Adding a time periodic perturbation to a Hamiltonian system has relevant effects. First of all, the number of degrees of freedom is increased. Another consequence is that, under generic hypotheses, the equilibrium points of the RTBP system become periodic orbits with the same period as the perturbation, in this case the period of the Sun. As we will see in the paper, this is the case for the L_3 point of the Earth-Moon Bicircular problem. As a curiosity, we note that triangular points are replaced by three periodic orbits; two stables and one unstable (the occurrence of three periodic orbits is due to the size of the perturbation, see [SGJM95, JCFJ18]).

1.1 Motivation and main results

It is well-known that the L_3 equilibrium point in the RTBP has stable and unstable manifolds that approach the small primary and give rise to a horseshoe structure [BO06]. The invariant manifolds related to the family of Lyapunov periodic orbits have transversal intersections, see [TSdSS14] for more details.

As we will discuss in Section 2.1, in the Bicircular model the point L_3 of the RTBP is replaced by a periodic orbit, with the same period as the Sun. The stability of this orbit is of saddle×centre type. This means that, under generic hypotheses, there exist a Cantor family of quasi-periodic orbits that is born in the centre direction. These quasi-periodic trajectories come from the family of periodic Lyapunov orbits of L_3 in the RTBP: the periodic orbits whose frequency satisfies a suitable Diophantine condition become quasi-periodic with two basic frequencies, the one of the Sun and the one they already had (see [JV97] for details). Roughly speaking, it can be said that the effect of the Sun is to "shaken" (periodically) the Lyapunov family of periodic orbits of L_3.

These quasi-periodic solutions are of saddle type so each of them has a stable and unstable manifolds. As each quasi-periodic solution fills densely a torus of dimension two, each manifold is of dimension three. As the family of tori is one parametric (with very small holes due to resonances), from a practical point of view the union of the, say, stable manifolds of all the tori is a fourth dimensional object that separates the fifth dimensional phase space and, hence, it organises the flow near L_3. In Section 2.2 we have computed this family of invariant tori, and in Sections 2.3 and 2.4 we have approximated the corresponding invariant manifolds. It is remarkable that these manifolds behave differently in the BCP than in the RTBP. In particular, they connect the two primaries and also connect them with the outside system.

Trajectories that enter and leave the system passing through L_3 may give us an insight about Near Earth Objects (NEO) dynamics. Previous works have pointed out the role of L_1 and L_2 and their associated invariant manifolds to explain their behaviour near the Earth-Moon system. Hou et al. explain in [HXSW15] that the typical way for a NEO to enter our system is first through Sun-Earth L_1 and L_2, and secondly, through Earth-Moon L_1 and L_2 for low energy trajectories, or directly without passing through any equilibrium point for high energy trajectories. Many other authors have also analysed these two collinear points for this purpose, for example, [SNU18] [LRMG14]. However, as far as we know, none of them have pointed to L_3, in spite of having the same kind of stability. One of the reasons why L_3 dynamics is not so popular could be its high energy, that makes it impossible for trajectories to enter and leave the system when considering the RTBP model.

One of the applications of this research is to lunar meteorites, which are meteorites originated on the Moon. They are thought to have their origin in the impacts that the Moon suffers every year. When an object impacts on the Moon surface with enough energy, a crater is produced. If the velocity of the crater ejecta is higher than the lunar escape velocity (≈ 2.38 km/s), they get free from the Moon gravity and become lunar meteorites travelling through space, being able to reach the Earth. In [GBDL95], Gladman et al. perform numerical simulation of a big number of initial conditions at the Moon surface for velocities in the range $[2.3, 3.5]$ km. There, they argue that a four body problem needs to be implemented to integrate initial conditions, due to the important effect Sun has on them.

Concerning how lunar meteorites reach the Earth, there are clear ideas of how the meteorites leave the Moon, and numerical computations supporting these ideas can be found in [GBD$^+$96]. There are also reliable physical procedures to analyse the time they have spent in space. However,

the geometrical mechanism behind this transport is not fully understood. As far as we know, no invariant object in the Earth-Moon vicinity is known to play a crucial role in their behaviour. In Section 3.1 we show that the invariant manifolds of the quasi-periodic orbits near L_3 in the BCP model are a mechanism for this transport.

Another application of the results in this paper is to give a new mechanism for a NEO to enter/leave the Earth-Moon system. In Section 3.2 we have followed the part of these manifolds that enters/leaves the system to characterise, by its orbital elements, the orbits around the Sun that are close to these manifolds.

There are also other reasons to study the dynamics near L_3, for instance its potential astronautical applications. The fact of being far from the Earth makes its position geometrically profitable to make astronomical measurements. So it would be interesting to place some station in L_3 vicinity for this end. In fact, it also would be very cheap, since the fuel consumption for the station keeping at L_3 is estimated about some cm/s per year, the same for L_4 and L_5, while the costs for doing so at L_1 and L_2 ascend to hundreds of m/s per year, [FV04].

In [TFR$^+$10], authors propose spacecraft trajectories to Sun-Earth L_3 point, motivated by the vast number of applications. However, we have not found many works proposing missions to Earth-Moon L_3 equilibrium point; the reason is again the energy level at which L_3 is placed and hence the high costs to get there. On the other hand, it is quite easy to leave the Earth-Moon system once you are in this region, so an space station there is also interesting as a gateway to Solar System missions.

Finally, as some stable invariant manifolds of L_3 tori collide with the Earth (hence, they intersect parking orbits), which means that a transfer to these regions can be done by a single manoeuvre, injecting the spacecraft on the stable manifold of the region around L_3 (see[LNJ20] for more details).

2 Invariant objects near L_3 in the BCP model

We recall that the effect of the Sun in the BCP introduces time-dependency to the equations of motion. In this situation it is usual to use the Poincaré section defined by the flow at time the period of the Sun $T = 2\pi/\omega_s$. In this case, the Poincaré map P_T is a diffeomorphism of an open domain of $\mathbb{R}^n$ into itself, where n is the dimension of the dynamical system; in this case $n = 4$ as we consider the system to be defined on the horizontal plane. In following sections, we make use of this Poincaré map in order to simplify computations. Notice that dynamical equivalents (periodic orbits of period T) are seen as fixed points of P_T.

In this section we also summarise the numerical methods used to compute invariant objects near L_3. First, in Subsection 2.1, we focus on the periodic orbit replacing L_3 in the BCP. Then, in Subsection 2.2 we describe the computation of invariant tori and in Subsection 2.3 their stability is analysed. Finally, Subsection 2.4 is devoted to the approximation of their invariant manifolds. All the numerical integrations have been done by means of Taylor methods [JZ05].

2.1 Dynamical equivalent for L_3 in the BCP

To apply a continuation method from the RTBP to the BCP, it is usual to add a parameter ε to (2),

$$H_\varepsilon = H_{RTBP} + \varepsilon \hat{H}_{BPC},$$

so that when $\varepsilon = 0$ we have the RTBP and when $\varepsilon = 1$ we have the BCP. Let us call P_ε the Poincaré map defined by the flow at time T for this Hamiltonian H_ε. It is clear that the L_3

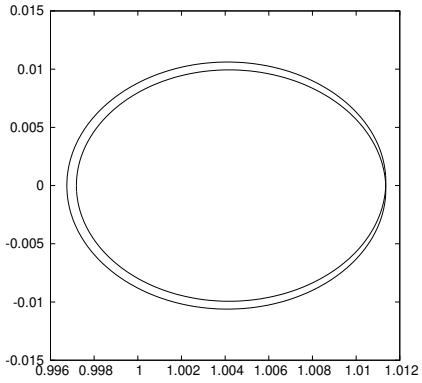

Figure 2: Periodic orbit replacing L_3 in the BCP, in the XY-plane.

point of the RTBP is a fixed point of P_ε for $\varepsilon = 0$. We continue this fixed points for ε going from 0 to 1, and no bifurcations occur. Figure 2 shows the resulting periodic orbit for $\varepsilon = 1$, that plays the role of L_3 in the BCP. The type of stability of the orbit remains the same as for L_3, centre×saddle. For $\varepsilon = 1$, the unstable eigenvalue of the fixed point that plays the role of L_3 is $\lambda_u \approx 3.372815841682823$.

It is important to mention that the reason for performing the continuation was to clarify that no bifurcation of the periodic orbit takes place, as it happens for L_4 and L_5, [SGJM95, JCFJ18]. Otherwise, the computation of this orbit could have been simply performed directly for the BCP (that is, $\varepsilon = 1$) and looking for the fixed point by means of a Newton method.

2.2 Invariant tori

In this section we discuss the numerical computation of the Lyapunov family of invariant tori near L_3. The methods we have used are explained in [CJ00] and [GJ04] and we refer to these references for deeper explanations.

Each torus of the family of invariant tori growing from the periodic orbit that replaces L_3 has two frequencies: the frequency of the Sun, plus another one which is different for each torus and it is close to the normal frequency of the periodic orbit. As the Solar frequency is known, we use the Poincaré map corresponding to the period of the Sun, P_T, to reduce this dimension for all the tori in the family. As a result, what we numerically compute is a family of invariant curves, such that every curve is characterised by a frequency denoted by ω. So, when applying the map P_T to one of the invariant tori of the family, we should see the same curve rotated a quantity equal to ω. This idea is expressed by the invariance equation, that must be satisfied by each of the invariant curves of the family. Let us write this in a more precise form.

Let $\varphi(\theta)$ be a parametrization of the curve in terms of an angle $\theta \in [0, 2\pi]$, where we assume that $\varphi(\theta)$ belongs to the space of continuous functions $C(\mathbb{T}^1, \mathbb{R}^4)$, and let $P_T(\varphi(\theta))$ be its image after a solar period. Then, the invariance equation is written as follows,

$$\varphi(\theta + \omega) = P_T(\varphi(\theta)). \tag{3}$$

The discretization of an invariant curve is performed by using a truncated Fourier series,

$$\varphi(\theta) \approx a_0 + \sum_{k=1}^{N} a_k \cos(k\theta) + b_k \sin(k\theta),$$

where N is the number of Fourier modes and a_0, a_k, b_k are the Fourier coefficients (that belong to $\mathbb{R}^4$). Therefore, what we will do is to use the invariance equation to find the set of coefficients for each curve.

For each curve there is a total of $4(2N+1)+1$ unknowns: $(2N+1)$ Fourier coefficients with 4 coordinates each and the frequency ω. A Newton method is applied in order to find the values for these unknowns that satisfies the invariance equation. Note that, as the parametrization is not unique (if $\varphi(\theta)$ is a parametrization then, for any α, $\varphi(\theta+\alpha)$ is a different parametrization of the same curve), an extra condition is needed. This makes a total of $4(2N+1)+2$ conditions.

For the moment being, let us assume that we have selected a suitable value of N (we will come back to this point later on). Let us consider the mesh $\theta_i = \frac{2\pi i}{2N+1}$, $0 \le i \le 2N$, and let us impose the invariant equation (3) on this mesh to produce $4(2N+1)$ conditions. We add an equation to fix one coordinate when $\theta = 0$, for example x plus another equation to fix another coordinate, for example y (in other words, when fixing these two coordinates we are looking for the invariant curve that goes through a certain point of the positions plane (x, y)). With this, the number of equations is $4(2N+1)+2$ for $4(2N+1)+1$ unknowns, and the system of equations is rectangular, although there is a redundant equation due to the lack of unicity of the parametrization. This is not a problem at all because the pivoting strategy used by the linear solver during the Newton iterations detects and removes the redundant equation.

To start the numerical continuation of the family we find first two invariant curves very close to the periodic orbit. This is done by choosing the x and y coordinates of the seed φ of the Newton method as $\varphi(\theta) = p + \delta(v_r \cos(k\theta) + v_i \sin(k\theta))$, where p is the point found for the periodic orbit replacing L_3 at $t = 0$, $v_r + \sqrt{-1}v_i$ is the eigenvector corresponding to the centre and δ is an small distance from the point p to the invariant curve, that has been chosen as $\delta = \{10^{-3}, 2\times 10^{-3}\}$. For more details concerning to the computation of these initial curves, we refer the reader to [GJ04].

Once the first two curves are obtained, a continuation method is applied to compute the Lyapunov family of invariant curves that emanates from the fixed point corresponding to the periodic orbit that replaces L_3. To have a uniform distribution of points[1] in the continuation curve , we ask to the new point in the continuation curve, φ_j, to be at distance δ of the previous point, φ_{j-1},

$$\|\varphi_j - \varphi_{j-1}\|^2 + (\omega_j - \omega_{j-1})^2 = |a_0^{(j)} - a_0^{(j-1)}|^2 + \sum_{k=1}^{N} \left(|a_k^{(j)} - a_k^{(j-1)}|^2 + |b_k^{(j)} - b_k^{(j-1)}|^2 \right) + (\omega_j - \omega_{j-1})^2 = \delta^2.$$

This condition replaces the condition of fixing the value of the y coordinate at $\theta = 0$. The seed for the Newton method is obtained by linear extrapolation from the last two points, φ_{j-1} and φ_{j-2}. If more than 4 steps of Newton method are required, the step of continuation δ is decreased.

The error of the invariant curve is estimated by checking the invariance condition (3) on a much finer mesh, say 100 times finer. The maximum difference gives an estimation of the error of the computed curve,

$$E(\varphi, \omega) = \max_{\theta \in \mathbb{T}^1} |\varphi(\theta + \omega) - P_T(\varphi(\theta))|.$$

If this value is bigger than a prescribed threshold (we have used 10^{-10}), the number of Fourier modes (i.e., the value of N) is increased.

[1] As it is usual in a continuation scheme, we refer to a single curve as a point in the family of invariant curves.

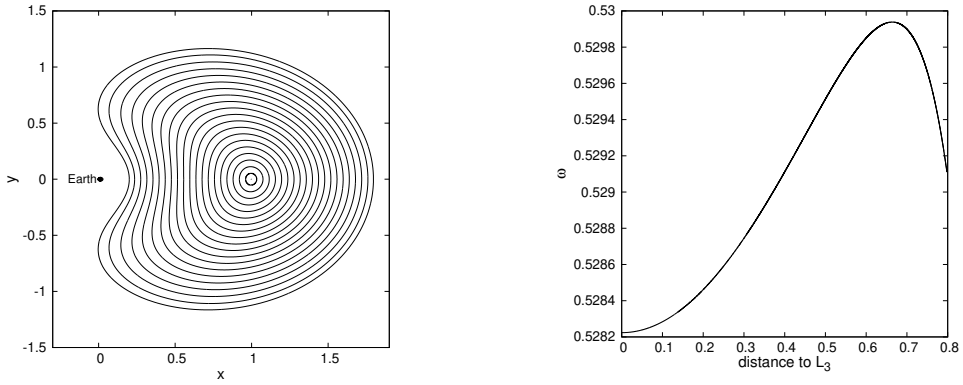

Figure 3: Left: family of invariant curves. Right: variation of the rotation number along the family.

Following the procedure explained above, we have been able to compute the family of invariant curves until a distance of 0.8 (as a measure of distance we use the difference between the x coordinate of the curve at the left intersection point with the x axis) from the fixed point that corresponds to L_3. With this definition of distance we can also say that the most exterior torus of the family is at a distance of 0.2 from the Earth, as shown in Figure 3 (left). Invariant tori at this distance are already covering a considerable region around L_3, so we have decided to stop the continuation here.

The computations have been started using $N = 25$ Fourier modes and finished using $N = 211$ (we recall that this value is adjusted automatically by the algorithm). In Figure 3 (right) we show the value of the frequency ω for the invariant curves according to their distance to L_3.

2.3 Stability of invariant tori

Once we have the invariant curves and their frequencies, we study the linear normal behaviour around them. As usual, we take an infinitesimal displacement, $h \in \mathbb{R}^4$, from the curve and look at its image by the Poincaré map,

$$P_T(\varphi(\theta) + h) = P_T(\varphi(\theta)) + D_x(P_T(\varphi(\theta)))h + O(\|h\|^2).$$

The linear normal behaviour around the invariant curves is therefore described by this dynamical system (also known as linear quasi-periodic skew product),

$$\begin{cases} \bar{\phi} = A(\theta)\phi, \\ \bar{\theta} = \theta + \omega, \end{cases} \tag{4}$$

where $A(\theta) = D_x(P_T(\varphi(\theta)))$. The system (4) is said to be reducible is there exists a continuous change of variables $\phi = C(\theta)\chi$ such that (4) becomes

$$\begin{cases} \bar{\chi} = B\chi, \\ \bar{\theta} = \theta + \omega, \end{cases} \tag{5}$$

where matrix $B = C^{-1}(\theta + \omega)A(\theta)C(\theta)$ does not depend on θ. Then, the stability of (4) follows immediately from the eigenvalues of matrix B in (5). In [Jor01] it is shown that these eigenvalues

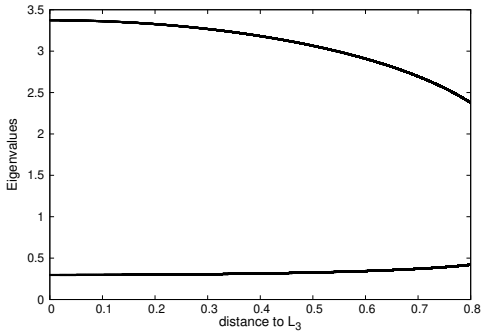

Figure 4: Hyperbolic eigenvalues w.r.t. the distance of the invariant curve to L_3.

can be found analysing the following generalised eigenvalue problem (GEV),

$$A(\theta)\psi(\theta) = \lambda\Gamma_\omega\psi(\theta), \tag{6}$$

where $(\lambda, \psi) \in \mathbb{C} \times (C(\mathbb{T}^1, \mathbb{C}^4) \setminus \{0\})$, and Γ_ω is the operator $\Gamma_\omega : \psi(\theta) \in C(\mathbb{T}^1, \mathbb{C}^4) \mapsto \psi(\theta + \omega) \in C(\mathbb{T}^1, \mathbb{C}^4)$. Using the same discretization used for the invariant curves, we compute the eigenvalues and eigenvectors (eigenfunctions) in (6). The discretized problem has dimension $4(2N+1) \times 4(2N+1)$ and this implies that we obtain $4(2N+1)$ eigenvalues. They are disposed in circles of radius $\{\lambda_s, 1, \lambda_u\}$, where the subindex s means stable and u, unstable (due to the Hamiltonian structure, we have that $\lambda_s = \lambda_u^{-1}$). Not all the eigenvalues have the same accuracy, so we select the most accurate ones to obtain the stability of the invariant curves and, from the eigenfunctions, the linear approximation to their stable and unstable manifolds. See [Jor01] for details on this procedure.

The evolution of eigenvalues of the family of invariant curves as we move away from L_3 is shown in Figure 4. We note that, as the invariant curves get further away, the unstable eigenvalue becomes smaller.

2.4 Invariant manifolds of invariant tori

The saddle part of each torus produces two invariant manifolds, one stable and one unstable. Stable invariant manifolds, W_s, are defined by the set of points that are sent towards the invariant tori forward in time, while unstable invariant manifolds, W_u, are defined by the set of points that are sent towards the tori backwards in time. In the previous section we have computed, for each invariant curve φ, two hyperbolic eigenvalues $\lambda_{s,u}$ and two eigenfunctions $\psi_{s,u}$ of (6). Note that, for $h \in \mathbb{R}$ small and any θ, they satisfy

$$P_T(\varphi(\theta)+h\psi_{s,u}(\theta)) = P_T(\varphi(\theta))+hD_xf(\varphi(\theta))\psi_{s,u}(\theta)+O(h^2) = \varphi(\theta+\omega)+h\lambda_{s,u}\psi_{s,u}(\theta+\omega)+O(h^2),$$

which means that

$$(\theta, h) \mapsto \varphi(\theta) + h\psi_{s,u}(\theta),$$

is a parametrization of the linearization of the manifolds of the invariant curve φ. For h small, this is an approximation of the true invariant manifold with an error of order h^2. To obtain a more global approximation to the manifold we follow the ideas in [Sim90]. First, we define a small displacement h_0 (we have used 10^{-5} or 10^{-6}, so that the error of the linear approximation

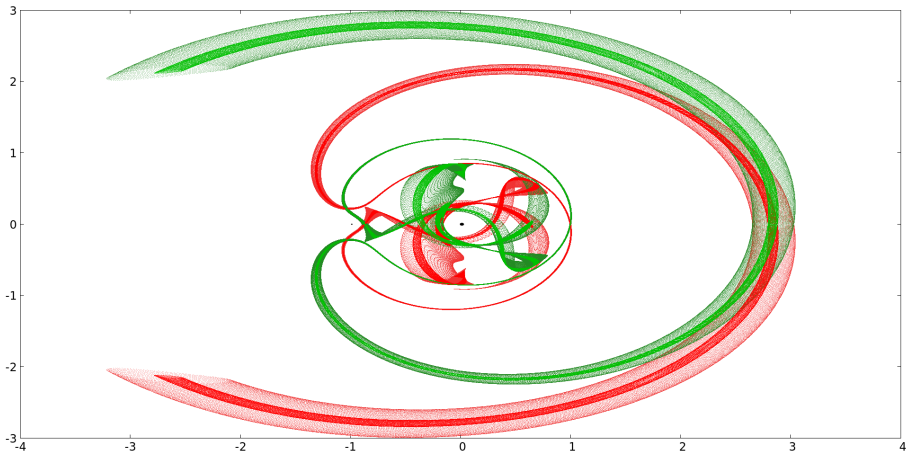

Figure 5: Stable (green) and unstable (red) invariant manifolds corresponding to two invariant curves, in the XY-plane. See the text for more details.

is of the order of 10^{-10}), and then we choose $h \in [h_0, h_0\lambda_u]$ (or $h \in [h_0, h_0/\lambda_s]$) so that $(\theta, h) \mapsto \varphi(\theta)+h\psi_{s,u}(\theta)$ is a parametrization of a fundamental set (in this case, a cylinder) on the invariant manifold, that spans the whole manifold by iteration under the Poincaré map P_T. Hence, to globalise the manifold, we have defined a equispaced mesh of M_1 values of h, and mesh of M_2 equispaced values of θ to construct a mesh of M_1M_2 points on the manifold that we propagate forward to span the unstable manifold and backwards to span the stable manifold. We note that we have to use h and $-h$ to have both "sides" of the manifold.

During the propagation of the orbits we check at every step of the integration if they have reached some of the primaries or if they have left the system. Leaving the system has been defined as being at a distance from the Earth-Moon barycentre larger than 10 Earth-Moon distances. At the moment that some orbit reaches the Earth or Moon, a Newton method is applied to refine the coordinates at which the orbit reaches their surfaces. This will be used later on.

3 Transport in the BCP

It is well known that the invariant manifolds of L_3 in the RTBP approach the small primary giving rise to horseshoe-like motions [BO06, SSST13]. As we will see, in the BCP the invariant manifolds of the tori near L_3 display a shape that reminds that of the RTBP, but with important differences. In particular, in the BCP the motion is not restricted to an energy level so that the manifolds fill a larger region of configuration space and even they move far away from the Earth-Moon system.

In Figure 5, invariant manifolds corresponding to two invariant tori (one at distance 1.3974×10^{-3} from L_3 periodic orbit, and another one at 5.5857×10^{-3}) are shown together to illustrate the shape of the manifolds for different tori. The trajectories correspond to the flow, not to the Poincaré map. For reference, Earth and Moon are also included in the figure as black circles of proportional radius.

As expected, it takes some Earth-Moon revolutions to leave L_3 neighbourhood. This is shown in Figure 6, where the manifolds of the curve at 1.3974×10^{-3} from L_3 are plotted for different

integration times. Images on the right column are the same as those on the left, but making a zoom around the primaries in order to show how some of the orbits reach them. The integration time for the first (upper) image is meaningless since it depend on the initial distance to the invariant torus. The following images are separated in time just by one Earth-Moon revolution. Note that the manifolds reach not only the Moon, but also the Earth. As a side comment, the reversing symmetry of the BCP mentioned in the introduction is now easy to observe: the stable manifold can be obtained from the unstable one by changing y by $-y$ and p_x by $-p_x$.

Next we perform massive numerical simulations to explore the evolution of the invariant manifolds for the computed family of invariant tori. The results show that most of the computed trajectories on the unstable manifolds (43.27%) leave the Earth-Moon system, a big amount of them (21.69%) go to the Moon and a smaller number (2.67%) go to the Earth. Due to the reversing symmetry, a 43.27% of trajectories on the sable manifold come from outside the Earth-Moon system, a 21.69% come from the Moon and a 2.67% come from the Earth. The remaining trajectories keep moving around the system without colliding with the primaries or escaping for the whole simulation.

In order to display the rich dynamics given by these invariant manifolds, let us discuss first how we introduce coordinates on them. As it has been discussed in the previous section we parametrize a fundamental region (a cylinder) of the, say, unstable manifold for an invariant curve φ as

$$(\theta, h) \in [0, 2\pi] \times [h_0, \lambda_u h_0] \mapsto \varphi(\theta) + h\psi_u(\theta).$$

Note that, in fact, we have two parametrizations of this kind, one for $h_0 > 0$ (the "positive piece" of the manifold) and another one for $h_0 < 0$ (the "negative piece"). We have used a mesh of 1000 equispaced points on $[0, 2\pi]$ and 1000 equispaced points on $[h_0, \lambda_u h_0]$ to produce 10^6 initial conditions for each piece of each unstable manifold (and similarly for the stable manifolds). We have coloured each couple (θ_i, h_j) according to the fate of the orbit that they genereate: yellow colour corresponds to escaping the Earth-Moon system, purple to collision with the Earth, red to collision with the Moon and black to those trajectories that move along the system without neither crashing nor escaping during the simulation time. Horizontal axis is taken as the angle along the curve $\theta \in [0, 2\pi]$ and the vertical one corresponds to the height of the fundamental domain, that is different for each curve, so we have scaled it to $[0, 1]$. Figure 7 shows several colour maps corresponding to the four pieces of the manifolds of an invariant curve close to L_3(at 3.3351×10^{-2} from L_3). The presence of the symmetry when inverting the time is easily recognisable, which means that from now on we will only plot, say, unstable invariant manifolds. Figure 8 shows colour maps for several invariant curves at different distances from L_3. Note that the left side of each plot coincides with the right side, due to the periodicity of θ. The upper side is the result of applying the Poincare map to the bottom side, so they coincide except for a shift equal to the frequency of the invariant curve.

Looking at Figures 7 and 8 we can see how the aspect of the colour maps evolves with the invariant curve. In general, in the first images, red and yellow colours seem to predominate, while for the last images quantity of purple and black colours has clearly increased; except for the first images in Figure 7, where purple regions are well defined. This means that it is more likely for the Earth to be origin or destiny of the trajectories passing close to the invariant curves near L_3, or far away from it, than for intermediate curves. The opposite effect is observed for the Moon. However, both primaries have connections with invariant curves at any distance from L_3. For each of the curves we have counted how many initial conditions on the fundamental cylinder reach the Earth, the Moon, escape the system, or none of these. The percentages are collected in Table 2. The two columns in each category correspond to the two sides of the manifold.

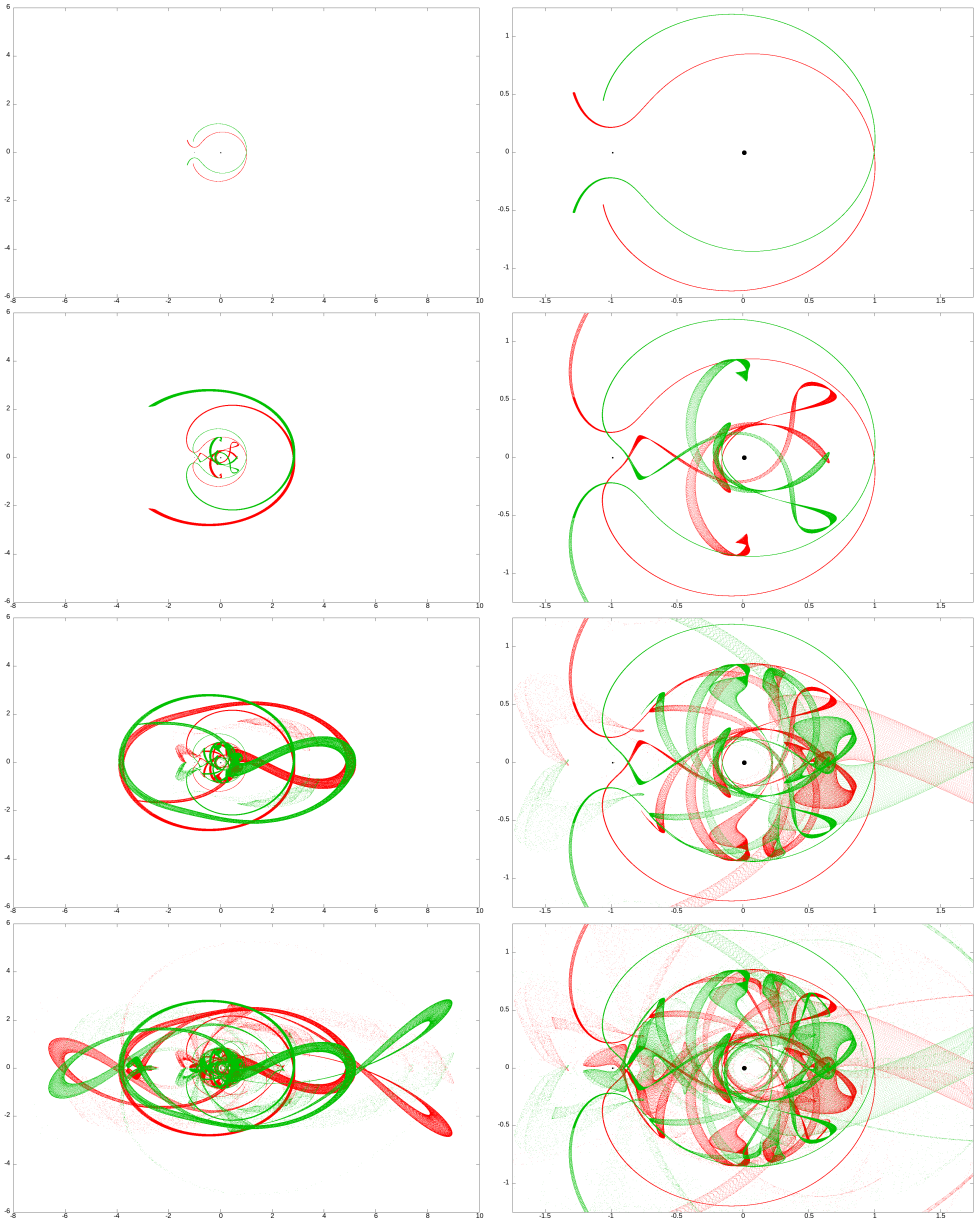

Figure 6: Invariant manifolds in the XY-plane of the curve at 1.3974×10^{-3} from L_3 for different times.

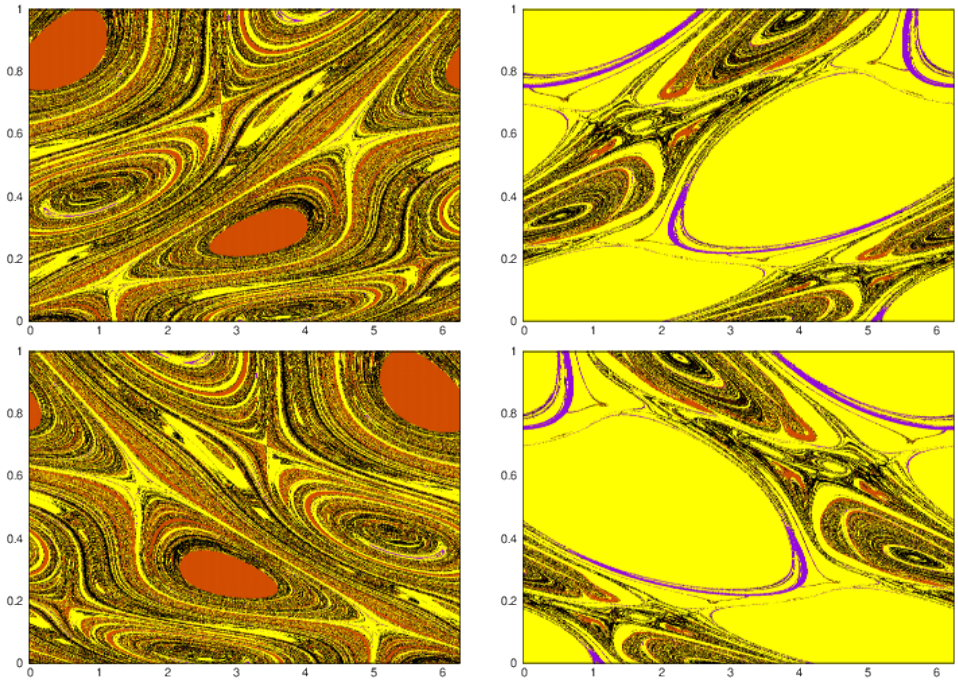

Figure 7: Fundamental cylinder of the invariant manifolds for an invariant curve at a distance 3.3351×10^{-2} from L3. Up, unstable manifolds. Down, stable manifolds. Left, positive piece. Right, negative piece. See text for more details.

Distance to L_3	Earth (%)		Moon (%)		Exterior (%)		Neither (%)	
1.3974×10^{-3}	1.93	6.93	12.19	0.19	49.63	92.20	36.27	0.68
3.3351×10^{-2}	1.73	3.75	26.85	5.09	39.11	77.38	32.30	13.93
1.9607×10^{-1}	1.76	1.68	29.08	31.19	43.54	41.72	25.63	25.42
3.0902×10^{-1}	1.92	1.50	24.30	22.35	45.68	53.50	28.21	22.69
4.9936×10^{-1}	2.55	1.88	18.71	20.04	39.04	39.19	39.71	38.89
5.7020×10^{-1}	2.57	2.19	15.42	18.78	36.20	37.93	45.82	41.10
7.4214×10^{-1}	5.61	3.89	12.56	14.71	35.52	39.53	46.31	41.87

Table 2: Percentages of the trajectories starting at fundamental cylinders that go to the Earth, Moon, outside system or neither, through the two directions of the unstable invariant manifolds for some invariant curves.

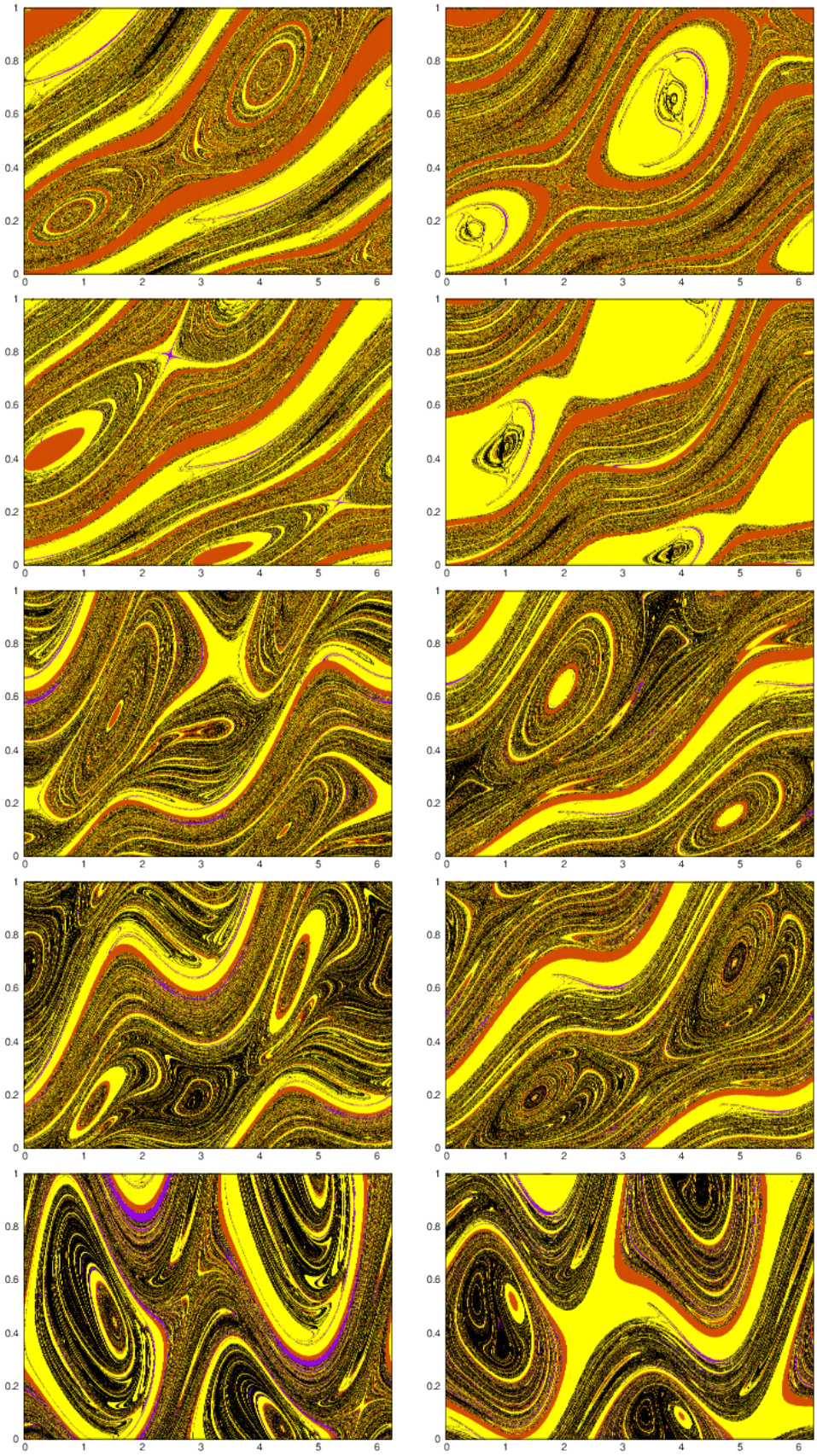

Figure 8: Fundamental cylinders for the two directions of the unstable manifolds of curves at distances to L_3, from up to down, 1.9607×10^{-1}, 3.0902×10^{-1}, 4.9936×10^{-1}, 5.7020×10^{-1} and 7.4214×10^{-1}.

The mix of colours in the maps in Figure 7 shows that a single invariant curve can be reached from several places and, starting at this quasi-periodic orbit, there are several possible destinations. These manifolds are the skeleton that organises the dynamics near L_3, and they provide multiple connections between Earth and Moon, and also allow to enter and exit the Earth-Moon system. In particular, it is remarkable that an asteroid entering the Earth-Moon system near these manifolds has more chances to impact on the Moon than on the Earth. Next Section contains numerical simulations around these manifolds to show the abundance of these connections.

3.1 Lunar meteorites

It is well known that some asteroids are frequently impacting on the Moon surface, being able to release material from the lunar surface. If the velocity at which this material is ejected from the Moon is high enough, they get free from the lunar gravity and start to move along the open space, becoming lunar meteorites. It is thought that some of these lunar meteorites reach the Earth what would explain why several stones, whose composition belongs to the Moon, are found on our planet.

In this section we study whether the invariant manifolds of the previous section can "guide" lunar meteorites to reach the Earth. The skeleton for these connections is defined by the subsets of the stable invariant manifolds can connect the Moon surface with a quasi-periodic orbit near L_3 whose unstable manifold reaches the Earth surface.

Let us start by computing the points (positions and velocities) at which stable manifolds reach the Moon surface, and the points at which unstable manifolds reach the Earth surface. It is remarkable that there is not a preferred time or point on the Moon surface for these orbits to start. Neither a prefer-ed time or point on the Earth surface for them to end. In order to illustrate this, in Figure 9 the histograms for the trajectories initial and final data. On the left of this figure, data corresponding to the Moon surface is presented; initial time, point along the surface and velocity. On the right, data of the destination of these trajectories, on the Earth surface, are also included; final time, point along the surface and velocity. Notice that time is parametrized in $[0, T]$, and the point along the primaries surfaces as circles of corresponding radius and angle in $[0, 2\pi]$. Ranges for velocities of the trajectories leaving the Moon are in $[2.25, 3.38]$ km/s, while for the velocities when they reach the Earth surface (neglecting atmosphere effects) is in the range $[11.00, 11.31]$ km/s. For velocities we do find some ranges that are preferred, or have higher possibilities. Vertical axis have been scaled such that they correspond to the probability percentage for each of the 100 bins.

Trajectories going from the Moon to the Earth can have very different shapes, depending on the invariant curve they approach during their journey. In Figure 10 two trajectories connecting Moon and Earth are shown; the left one is close to the invariant manifolds of a quasi-periodic orbit close to L_3 and the right one is close to the invariant manifolds of a quasi-periodic orbit far from L_3.

To see how likely is for a Moon ejecta to follow these trajectories we have performed a series of numerical simulations. To this end, for each intersection point of the stable manifolds with the Moon surface, we have modified the corresponding velocity module and direction maintaining its x and y coordinates, as well as the inital time (we recall that the BCP depends on time). A mesh of modules and angle directions for the velocities is created from the values of the trajectory.

The mesh is formed by 10^3 points in each direction (modulus and angle of the velocity vector) for a total of 10^6 points. Each of these points gives an initial condition that is integrated

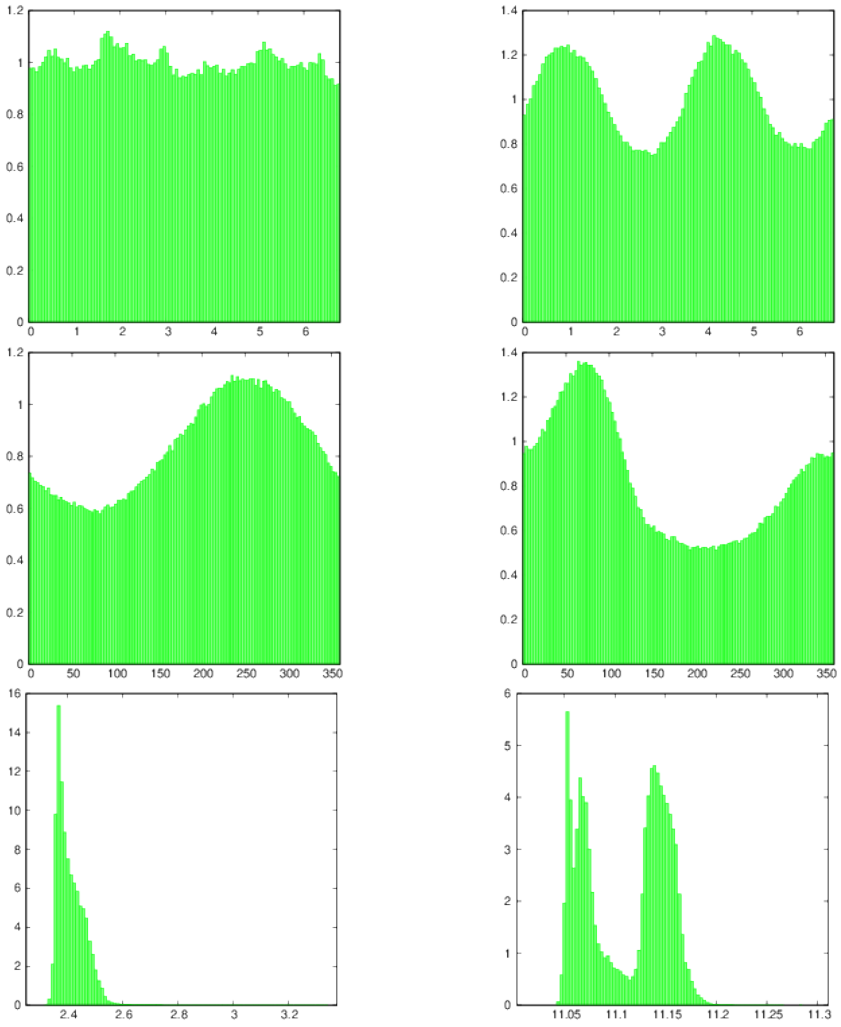

Figure 9: Left column contains histograms for the Moon; from up to down they show the time leaving the primary, the point of the surface at which it happens, and escape velocity. Right column contains similar histograms buy for the Earth. See the text for more details.

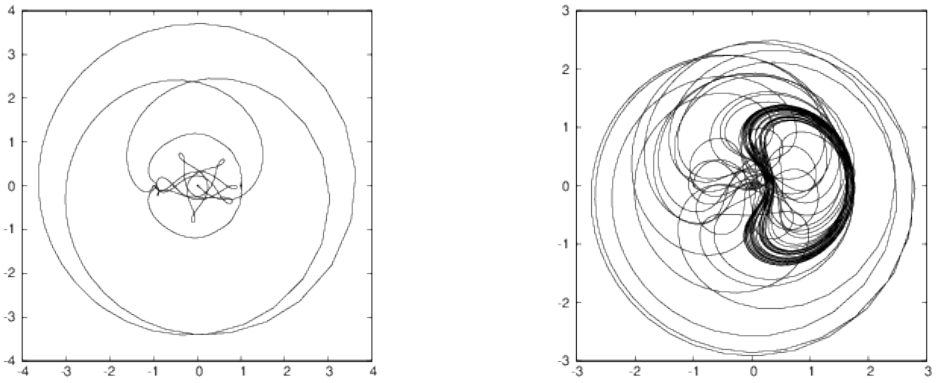

Figure 10: Two trajectories, in the XY-plane, connecting the Moon with the Earth. See the text for details.

Trajectory	1st	2nd	3rd	4th
ϑ	132.917506118	225.259626325	298.729423247	263.209360181

Table 3: Initial angular position of the Sun with respect to the Earth-Moon barycentre (ϑ) in degrees, for the trajectories in Figure 11.

during a maximum of 55 Earth-Moon revolutions; depending on their final destination a colour is assigned to them, see Figure 11. As in the colour maps from Section 3, yellow corresponds to trajectories that leave the Earth-Moon system, purple to those that reach the Earth and red colour to those that come back to the Moon. There are also a few trajectories in black colour that neither crash nor leave the system. The trajectory at the left of each colour map corresponds to an orbit which is extremely close to the invariant manifold and reaches the Earth (we note that, in a perfect computation with no errors, an orbit exactly on the manifold will accumulate to the quasi-periodic orbit without going anywhere else). Note that the plot axis have been adjusted differently for each trajectory.

In these maps we find a large variety of destinations for each of the trajectories starting on the Moon surface and near the stable manifold. We can see that only for higher velocities big areas of initial conditions leading to the Earth from the Moon are found. Also, it is quite visible that three of the four maps have a vertical red band on the left of the plot, the reason for this to happen is that those are trajectories with velocities below the Moon velocity escape, consequently they tend to fall again against the lunar surface. However, in the last map this red vertical band is not present, the reason may be the relative position of the Sun when the trajectory starts, that helps to escape Moon's gravity. In Table 3 the initial angular position of the Sun (ϑ, see Figure 1) for the four trajectories are shown. Notice that for the last trajectory, the initial position of the Sun is almost vertically above the primaries.

A last comment on this section is devoted to transfers from the Earth to the Moon. We do not consider ejecta from Earth travelling to the Moon since the effect of Earth's atmosphere would ask for extremely high speeds but the transfer from an orbit around the Earth to the Moon has undoubtedly astronautical interest. Therefore, we can use the same strategy but starting at some distance from the Earth surface, for instance at some Parking Orbit (PO). If a quasi-periodic orbit has a stable invariant manifold crossing a PO and an unstable manifold

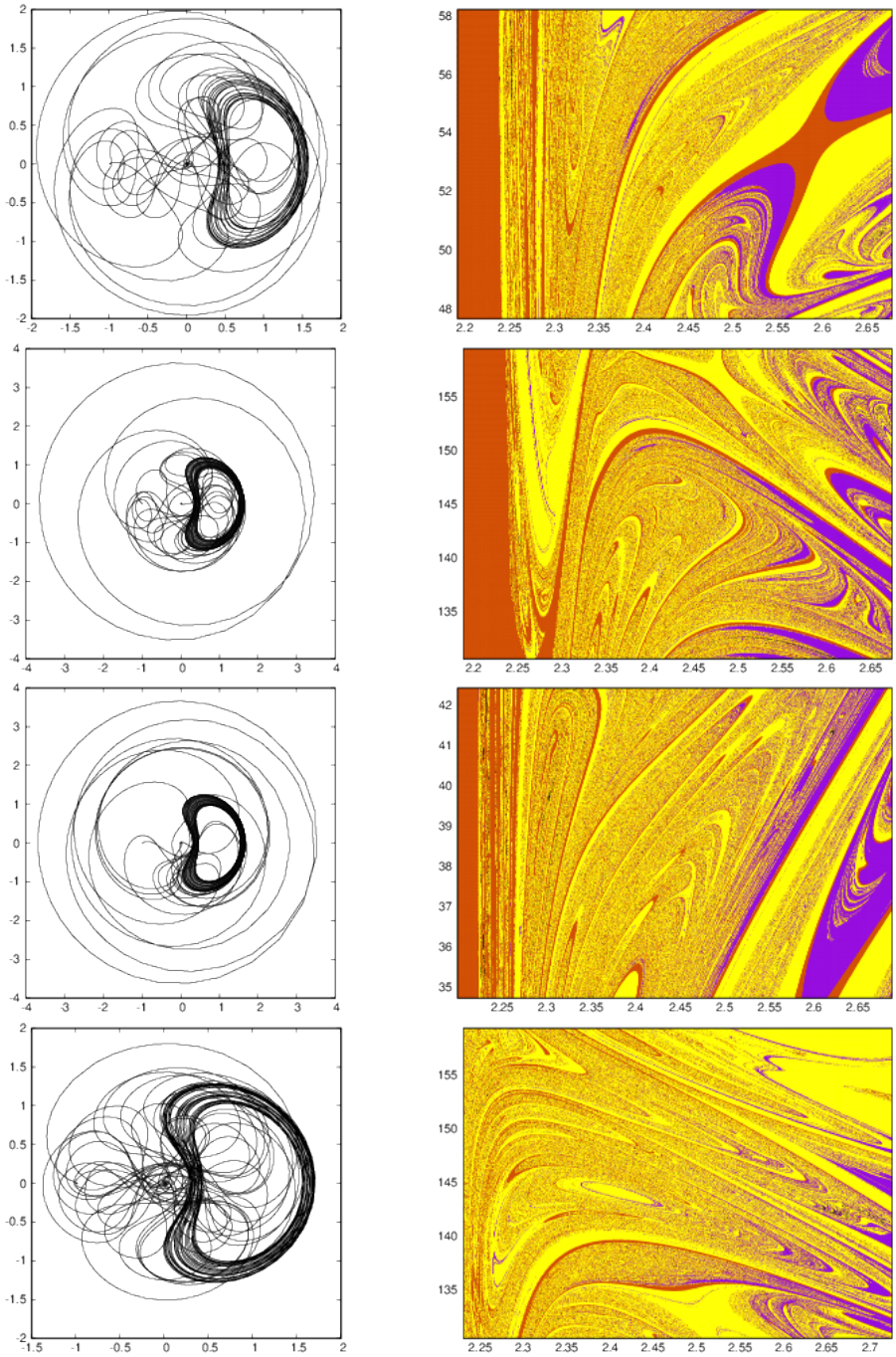

Figure 11: Left, trajectories connecting the Moon with the Earth, in the XY-plane. Right, destination colour maps when modifying trajectories velocities; horizontal axis corresponds to the velocity module (km/s) and vertical to the angle direction (degrees). The trajectory on the left corresponds to the centre point of the map at the right. See the text for more details.

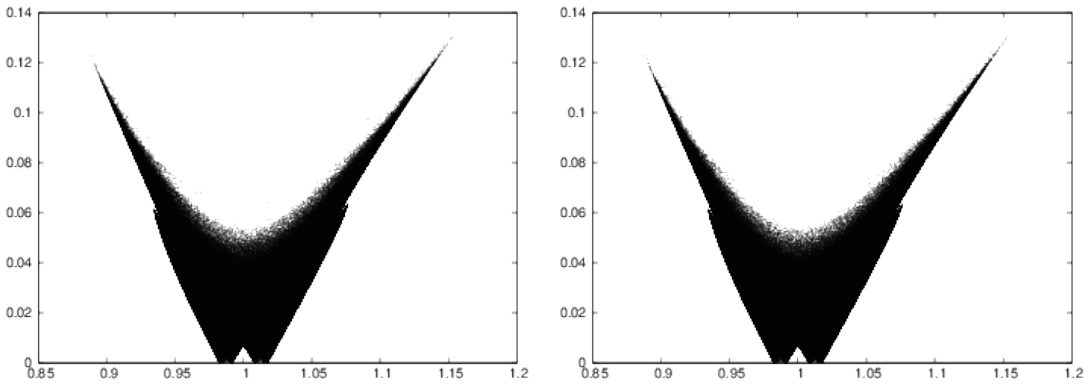

Figure 12: Horizontal axis corresponds to semi-axis (in astronomical units), and vertical to eccentricity. Orbital elements for orbits entering (left) and leaving (right) the Earth-Moon system.

colliding with the Moon we can use this geometrical structure to go to the Moon by means of a single manoeuvre, which is a change of velocity Δv at the crossing point (in configuration space) of the PO with the stable manifold. We have done some estimations on the Δv costs for transferring to L_3 stable manifolds from a PO defined at 200 km from the Earth surface, and they show that minimum cost for some spaceship to make this manoeuvre is of 3.17 km/s; value near typical costs for leaving an PO at this distance to go to the Moon. We have not performed a deeper study in this direction, since it is not our goal in the present work. In [LNJ20] the costs for entering in one of these orbits are refined and a transfer is proposed from a PO to the Earth-Moon triangular points through the neighbourhood of L_3. A similar strategy could be used to reach the Moon.

3.2 Entering and leaving orbits

Due to Sun gravitational attraction, when a particle reaches a distance far enough from the Earth-Moon barycentre, it is captured by the Solar gravitational field. Consequently, unstable manifolds that overcome this distance are said to leave the Earth-Moon system, and stable ones, are said to enter in the system, both led by L_3 dynamics. To analyse the kind of trajectories that enter and leave the system, their orbital elements with respect to the Sun are computed. As the model treated here is planar, only semi-axis and eccentricity are obtained. Before computing the orbital elements, synodic coordinates are translated to inertial ones, with the origin set at Sun position.

In Figure 12 semi-axis and eccentricity are shown. Due to the time reversibility of the system, it is quite natural that the orbital elements corresponding to trajectories that have escaped the Earth-Moon system are similar to those corresponding to trajectories that will enter the system.

Granvik et al., [GVJ12], computed the capture probability for NEOs according to their orbital elements. If we compare their results with the orbital elements obtained with the Bicircular Problem (Figure 12), it seems that trajectories entering and leaving the Earth-Moon system described by BCP, are probably to happen in the real system.

Our results show that these entering manifolds connect, near L_3, with manifolds that go towards the Moon or the Earth, and viceversa. Moreover, we have observed trajectories that

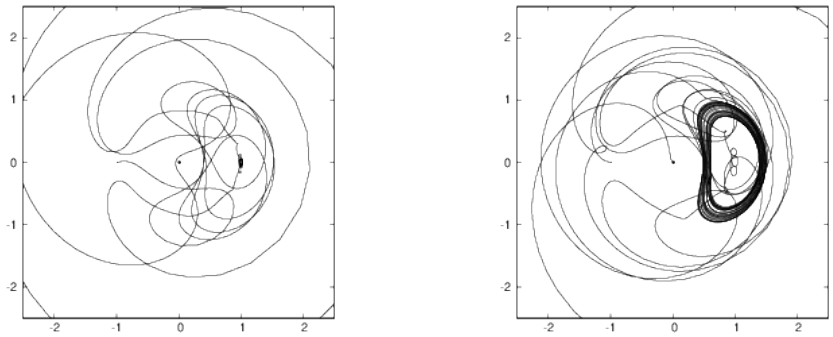

Figure 13: Trajectories that suggest intersections between the manifolds of different invariant curves.

enter in the Earth-Moon system after orbiting the Sun in an orbit outer than the one of the Earth (i.e., with semi-axis larger than $1AU$) and then leave the system to orbit around the Sun in an inner orbit than the Earth (semi-axis smaller than $1AU$). In the same way, the opposite transfer (from an inner orbit around the Sun to an outer one) can be led by L_3 dynamics. This behaviour reminds that of the quasi-satellites except for the fact here there is no inclination for the trajectories, [MIW$^+$06].

3.3 On the existence of heteroclinic orbits

Another phenomenon we have observed is that it seems that there exist intersections among manifolds of different quasi-periodic orbits near L_3. In Figure 13 (left) we can see an orbit that goes from the Moon surface to the outside system through a torus close to L_3, but it also seems to spin around a second torus. In Figure 13 (right), we can observe the opposite effect, for an orbit that goes from the Moon to the Earth. The study of these connections is left for another work.

4 Transport in a realistic model

The results concerning to the transport between Earth and Moon that we have obtained by analysing L_3 in the Bicircular Problem may explain the behaviour of lunar meteorites travelling to the Earth. Now we want to check these results in a more realistic model. To this end, we consider the Solar system as an N-body problem containing Sun, Earth, Moon and all the planets, with initial conditions provided by the JPL ephemeris DE405. The initial conditions for the particles are obtained by means of a change of coordinates from BCP to the the ecliptic system of reference, whose origin is placed at the Solar system centre of mass. Once the change is performed, we integrate every particle jointly with the Solar system as a restricted $(N+1)$-body problem. Let us see this with more detail.

4.1 Changes of coordinates

The change of coordinates applied here can also be found in [GLMS01]. Let R_E, R_M and b be the positions of the Earth, Moon and their barycentre at a given time, in ecliptic coordinates with origin at the Solar System barycentre. These values are provided by the JPL ephemeris.

Now, let a be the position of a particle in the adimensional BCP system and e its position in the ecliptical reference system. The relation between them is of the following type,

$$e = kCa + b, \tag{7}$$

where $k = \|R_E - R_M\|$ is the change of scale factor, C is an orthogonal matrix that gives the rotation between e and a coordinates and adding b means the translation of the origin. The rotation matrix C is composed by three unitary column vectors c_1, c_2 and c_3, defined as:

$$c_1 = \frac{R_E - R_M}{||R_E - R_M||}, \qquad c_3 = \frac{(R_M - R_E) \wedge (V_M - V_E)}{||(R_M - R_E) \wedge (V_M - V_E)||}, \qquad c_2 = c_3 \wedge c_1,$$

where V_E and V_M are the velocities of the Earth and Moon. Notice that the first vector marks the direction between the two primaries, the expression of the third one is the normalised angular momentum for Earth and Moon, and the second one is perpendicular to the other two giving an positively oriented reference frame. To transform velocities from the adimensional system ($\dot{a}$) to the ones in the ecliptical system ($\dot{e}$) we take derivatives with respect to time in (7),

$$\dot{e} = \dot{k}Ca + k\dot{C}a + kC\dot{a} + \dot{\vec{b}}. \tag{8}$$

Here $\dot{\vec{b}}$ is the velocity of the barycentre, and the derivative of the rotational matrix is performed by derivating every element of the three column vectors, what implies the accelerations of the Earth and the Moon, that are computed from the Newtonian equations of motion of the full Solar system.

It is important to realise that the relation between units of length between the two systems is given by the scale factor k. However, when we take derivatives with respect to time, that in the JPL model is given in days, we need to introduce the adimensional velocities ($\dot{a}$) in units of adimensional length over days.

4.2 Lunar meteorites

Every initial condition of the maps in Figure 11 has been translated to the ecliptical system by applying the change of coordinates given by (7) and (8). Notice that our coordinates in the BCP are four-dimensional, so initial vertical position and velocity in the adimensional system are zero. Also, each colour map corresponds to a different starting time (the angles in Table 3), that needs to be translated to modified Julian days (the time in the JPL ephemeris is measured in Julian days). Since time zero for BCP model corresponds to a lunar eclipse we have chosen as origin of time in the real system the first lunar eclipse of year 2000, which corresponds to the modified Julian day 20.1978749133 (day 0.0 corresponds to year 2000.0). Taking all this into account, we obtain the initial data for each point of the colour maps with the same units as in the JPL ephemeris.

The initial numerical simulations, with the same mesh of initial conditions as in the BCP, showed similar patterns but sometimes with a shift, mainly in velocities, and different in each case. For this reason we have enlarged the mesh to cover a larger set of initial data. The results are shown in Figure 14. An explanation of these shifts, different for each map (i.e. for each different time) may be given by the relative positions and velocities of the Earth and Moon at each time. This implies a different scale factor that can be translated into higher or lower velocities for the initial conditions, see Table 4. The last column in this table, $\sigma = \|\dot{e} - V_M\| - \|\dot{a}\|$ (in km/s), is a comparison of the initial velocities with respect to the Moon in the two reference

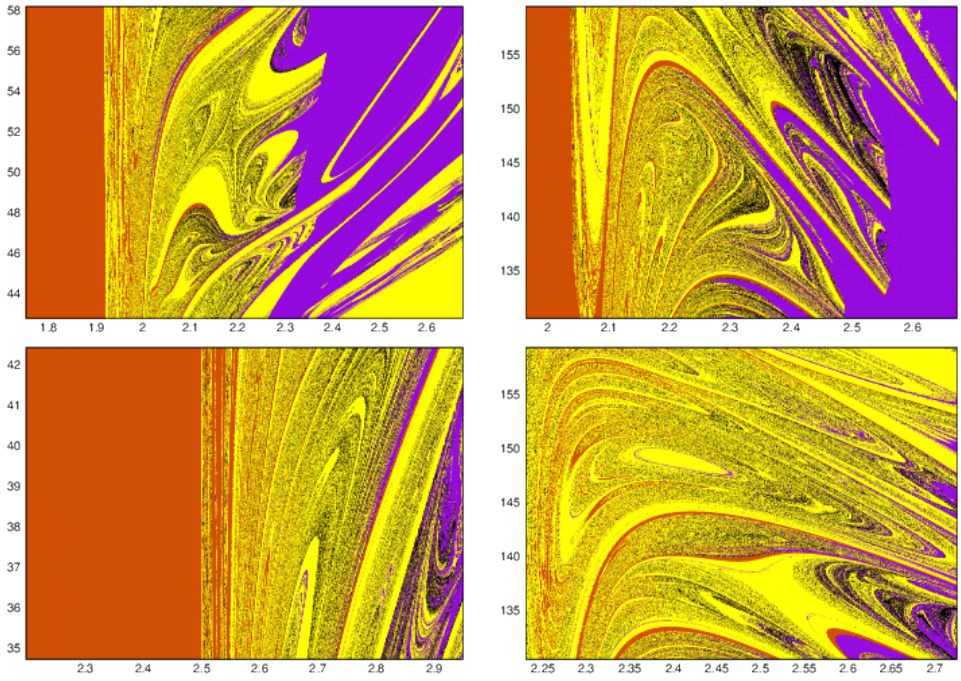

Figure 14: JPL results for the destination colour maps when modifying trajectories velocities; horizontal axis corresponds to the velocity module (km/s) and vertical to the angle direction (degrees). See the text for more details.

frames. Note that value of σ is correlated with the shift in velocities when comparing the colour maps in Figures 11 and 14. It is remarkable that for the time of the fourth map the relative positions of Earth, Moon and Sun are close enough to the (planar) BCP configuration so that we have not needed to widen the mesh to find the same patterns.

As a last check, the trajectories that leave the Earth-Moon system in those integrations (yellow colour in the maps), are characterised in terms of their orbital elements. Again, for the planar Bicircular model, only semi-major axis and eccentricity can be computed. For the realistic, all the orbital elements have been computed. Here we only include the semi-major axis, eccentricity and inclination values for the four maps, see Figure 15. Again, the plots for the BCP and for the real model are in good agreement.

5 Conclusions

This work focuses on the role of L_3 equilibrium point in the planar Earth-Moon system under the perturbation of the Sun. First, we have found the dynamical equivalent for this point in the Bicircular model. Then, the family of Lyapunov quasi-periodic orbits that emanates from L_3 has been numerically computed and its stability analysed. The computation of their stable and unstable invariant manifolds shows the existence of connecting orbits between Earth and Moon, and trajetories that enter and/or escape the Earth-Moon system. By means of numerical simulation, we have shown that these connections can be a mechanism for the transport of lunar ejecta to the Earth. We have tested these trajetories with a realistic model for the Solar system

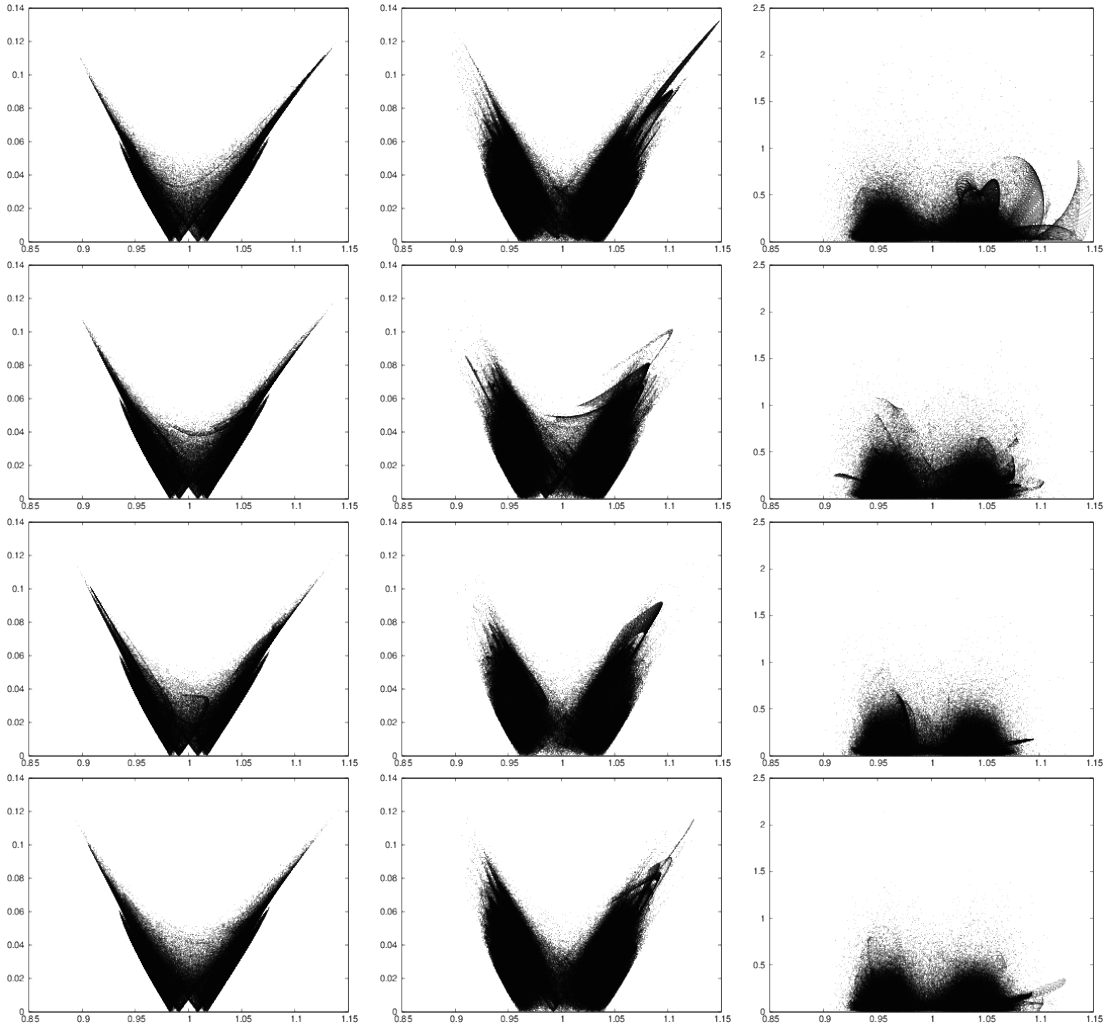

Figure 15: Orbital elements for the trajectories that leave the Earth-Moon system, corresponding to the four maps of initial conditions defined in Section 3.1 (from up to down), integrating them in the BCP (first column) and in a realistic N-body problem (other two). First two columns of graphs show eccentricity versus semi-major axis (astronomical units), and the last one the inclination (in degrees) versus semi-major axis.

Trajectory	k (km)	V_{EM} (km/s)	ω_{EM} (1/s)	e_z (km)	σ (km/s)
1st	404835.4469	0.9702	2.3964×10^{-6}	64623.3917	1.4039×10^{-1}
2nd	396750.5357	0.9923	2.5012×10^{-6}	16469.0752	6.2282×10^{-2}
3rd	369879.1465	1.0594	2.8641×10^{-6}	-2390.8644	-1.0638×10^{-1}
4th	384247.7345	1.0195	2.6533×10^{-6}	-517.1608	-1.3396×10^{-2}
BCP	384400.0000	1.0236	2.6628×10^{-6}	0.0000	--------

Table 4: Scale factor, relative Earth-Moon linear and angular velocities and vertical coordinate in the ecliptic system and BCP for the initial data of the four trajectories of Figure 11. Last row corresponds to the difference in the ecliptical velocity module for the particle relative to the adimensional one.

and the results are in good agreement with those of BCP. This means that these invariant objects of the BCP seems to provide a structure to guide Moon ejecta to the Earth. Moreover, the simulation in the real model of Moon ejecta escaping the Earth-Moon system is also in good agreement with the BCP results.

In the same way, these connections could be used to design a mission to the Moon starting at a Parking Orbit of the Earth. In addition, trajectories entering and leaving our system can give some insight in NEOs dynamics, in particular these manifolds connect orbits semi-major axis larger than 1 AU with orbits with semi-major axis smaller than 1 AU. All these phenomena, that appear naturally in this study, will lead us to deeper research, both in the case of natural orbits and in the case of orbits for astronautical applications.

Acknowledgements

This work has been supported by the Spanish grants PGC2018-100699-B-I00 (MCIU/AEI/FEDER, UE) and the Catalan grant 2017 SGR 1374. The project leading to this application has received funding from the European Union's Horizon 2020 research and innovation programme under the Marie Skłodowska-Curie grant agreement No 734557. B. Nicolás is supported by the Ministry of Economy, Industry and Competitiveness of Spain through the National Plan for I+D+i (MTM2015-67724-R) and through the national scholarship BES-2016-078722.

References

[BO06] E. Barrabés and M. Ollé. Invariant manifolds of L_3 and horseshoe motion in the Restricted Three-Body Problem. *Nonlinearity*, 19, 04 2006.

[Bro68] R. Broucke. Periodic orbits in the restricted three-body problem with Earth-Moon masses. Technical Report 32-1168, Jet Propulsion Laboratory, NASA, 1968.

[CJ00] E. Castellà and À. Jorba. On the vertical families of two-dimensional tori near the triangular points of the Bicircular problem. *Celestial Mech.*, 76(1):35–54, 2000.

[CRR64] J. Cronin, P.B. Richards, and L.H. Russell. Some periodic solutions of a four-body problem. *Icarus*, 3:423–428, 1964.

[FV04] D. Folta and F. Vaughn. A comprehensive survey of Earth-Moon libration orbits: Stationkeeping strategies and intra-orbit transfers. *Collection of Technical Papers - AIAA/AAS Astrodynamics Specialist Conference*, 1, 02 2004.

[GBD+96] B. J. Gladman, J. A. Burns, M. J. Duncan, P. Lee, and H. F. Levison. The exchange of impact ejecta between terrestrial planets. *Science*, 271(5254):1387–1392, 1996.

[GBDL95] B. J. Gladman, J. A. Burns, M. J. Duncan, and H. F. Levison. The dynamical evolution of lunar impact ejecta. *Icarus*, 118(2):302 – 321, 1995.

[GJ04] F. Gabern and À. Jorba. Generalizing the Restricted Three-Body Problem. The Bianular and Tricircular Coherent Problems. *Astron. Astrophys.*, 420:751–762, 2004.

[GLMS01] G. Gómez, J. Llibre, R. Martínez, and C. Simó. *Dynamics and mission design near libration points. Vol. I, Fundamentals: the case of collinear libration points*, volume 2 of *World Scientific Monograph Series in Mathematics*. World Scientific Publishing Co. Inc., 2001.

[GVJ12] M. Granvik, J. Vaubaillon, and R. Jedicke. The population of natural Earth satellites. *Icarus*, 218(1):262 – 277, 2012.

[Hua60] S.S. Huang. Very restricted four-body problem. Technical note TN D-501, Goddard Space Flight Center, NASA, 1960.

[HXSW15] X. Y. Hou, X. Xin, D. J. Scheeres, and J. Wang. Stable motions around triangular libration points in the real Earth-Moon system. *Mon. Not. R. Astron. Soc.*, 454(4):4172–4181, 2015. https://doi.org/10.1093/mnras/stv2216.

[JCFJ18] M. Jorba-Cuscó, A. Farrés, and À. Jorba. Two periodic models for the Earth-Moon system. *Front. Appl. Math. Stat.*, 4, 2018.

[Jor00] À. Jorba. A numerical study on the existence of stable motions near the triangular points of the real Earth-Moon system. *Astron. Astrophys.*, 364(1):327–338, 2000.

[Jor01] À. Jorba. Numerical computation of the normal behaviour of invariant curves of n-dimensional maps. *Nonlinearity*, 14(5):943–976, 2001.

[JV97] À. Jorba and J. Villanueva. On the persistence of lower dimensional invariant tori under quasi-periodic perturbations. *J. Nonlinear Sci.*, 7:427–473, 1997.

[JZ05] À. Jorba and M. Zou. A software package for the numerical integration of ODEs by means of high-order Taylor methods. *Exp. Math.*, 14(1):99–117, 2005.

[LNJ20] Y. Liang, B. Nicolás, and À. Jorba. Leverage L_3 to triangular libration points transfer in Sun-perturbed Earth-Moon system. Preprint, 2020.

[LRMG14] N. Lladó, Y. Ren, J.J. Masdemont, and G. Gómez. Capturing small asteroids into a Sun-Earth Lagrangian point. *Acta Astron.*, 95(Supplement C):176–188, 2014. https://doi.org/10.1016/j.actaastro.2013.11.007.

[MIW+06] S. Mikkola, K. Innanen, P. Wiegert, M. Connors, and R. Brasser. Stability limits for the quasi-satellite orbit. *Monthly Notices of the Royal Astronomical Society*, 369(1):15–24, 05 2006.

[SGJM95] C. Simó, G. Gómez, À. Jorba, and J. Masdemont. The Bicircular model near the triangular libration points of the RTBP. In A.E. Roy and B.A. Steves, editors, *From Newton to Chaos*, pages 343–370, New York, 1995. Plenum Press.

[Sim90] C. Simó. On the analytical and numerical approximation of invariant manifolds. In D. Benest and C. Froeschlé, editors, *Modern methods in celestial mechanics*, pages 285–330. Ed. Frontières, 1990. Reprinted at `http://www.maia.ub.es/dsg/2004/index.html`.

[SNU18] J.-P. Sánchez, R. Neves, and H. Urrutxua. Trajectory design for asteroid retrieval missions: A short review. *Frontiers in Applied Mathematics and Statistics*, 4:44, 2018.

[SSST13] C. Simó, P. Sousa-Silva, and M. Terra. Practical stability domains near $L_{4,5}$ in the restricted three-body problem: some preliminary facts. In *Progress and challenges in dynamical systems*, volume 54 of *Springer Proc. Math. Stat.*, pages 367–382. Springer, Heidelberg, 2013.

[TFR+10] M. Tantardini, E. Fantino, Y. Ren, P. Pergola, G. Gómez, and J. Masdemont. Spacecraft trajectories to the L_3 point of the Sun-Earth three-body problem. *Celestial Mech. Dynam. Astronom.*, 108:215–232, 11 2010.

[TSdSS14] M. O. Terra, C. Simó, and P. A. de Sousa Silva. Evidences of diffusion related to the center manifold of L_3 of the SRTBP. In *65th International Astronautical Congress, Toronto, Canada.*, 2014.